UNIVERSITYOF BIRMINGHAM

Measurement of road traffic brake and tyre dust emissions using both particle composition and size distribution data

Beddows, David C.S.; Harrison, Roy M.; Gonet, Tomasz; Maher, Barbara A.; Odling, Nicholas

Document Version
Publisher's PDF, also known as Version of record

[Link to publication on Research at Birmingham portal](#)

Measurement of road traffic brake and tyre dust emissions using both particle composition and size distribution data[☆],[☆☆]

David C.S. Beddows [a], Roy M. Harrison [a],[d],[*], Tomasz Gonet [b],[1], Barbara A. Maher [b], Nicholas Odling [c]

[a] National Centre for Atmospheric Science, School of Geography, Earth and Environmental Sciences, University of Birmingham, Edgbaston, Birmingham, B15 2TT, United Kingdom
[b] Centre for Environmental Magnetism & Palaeomagnetism, Lancaster Environment Centre, Lancaster University, Lancaster, LA1 4YQ, United Kingdom
[c] School of Geosciences, University of Edinburgh, Kings Buildings, West Mains Road, Edinburgh, EH9 3JW, Scotland, United Kingdom
[d] Department of Environmental Sciences, Faculty of Meteorology, Environment and Arid Land Agriculture, King Abdulaziz University, Jeddah, Saudi Arabia

ARTICLE INFO

ABSTRACT

Estimates of tyre and brake wear emission factors are presented, derived from data collected from roadside and urban background sites on the premises of the University of Birmingham, located in the UK's second largest city. Size-fractionated particulate matter samples were collected at both sites concurrently in the spring/summer of 2019 and analysed for elemental concentrations and magnetic properties. Using Positive Matrix Factorisation (PMF), three sources were identified in the roadside mass increment of the 1.0–9.9 μm stages of MOUDI impactors located at both sites, namely: brake dust (7.1%); tyre dust (9.6%); and crustal (83%). The large fraction of the mass apportioned to crustal material was suspected to be mainly from a nearby construction site rather than resuspension of road dust. By using Ba and Zn as elemental tracers, brake and tyre wear emission factors were estimated as 7.4 mg/veh.km and 9.9 mg/veh.km, respectively, compared with the PMF-derived equivalent values of 4.4 mg/veh.km and 11 mg/veh.km. Based on the magnetic measurements, an emission factor can be estimated independently for brake dust of 4.7 mg/veh.km. A further analysis was carried out on the concurrently measured roadside increment in the particle number size distribution (10 nm-10 μm). Four factors were identified in the hourly measurements: traffic exhaust nucleation; traffic exhaust solid particles; windblown dust; and an unknown source. The high increment of the windblown dust factor, 3.2 μg/m^3, was comparable in magnitude to the crustal factor measured using the MOUDI samples (3.5 μg/m^3). The latter's polar plot indicated that this factor was dominated by a large neighbouring construction site. The number emission factors of the exhaust solid particle and exhaust nucleation factors were estimated as 2.8 and 1.9 x 10^{12}/veh.km, respectively.

1. Introduction

Air pollution presents a major public health risk, ranking alongside cancer, heart disease and obesity, and poses the single greatest environmental risk to human health. As well as human health impacts, air pollution has implications for the natural environment and for the economy. In January 2019, the UK government committed to a Clean Air Strategy which sets out actions designed to achieve a reduction in particulate matter (PM) concentrations. Subsequent legislation commits the UK government to legal targets for future reduced concentrations of PM$_{2.5}$. On the international scene, the updated WHO guidelines (WHO, 2022) recommend challenging targets for concentrations of both PM$_{2.5}$ and PM$_{10}$. Non-exhaust emissions (NEEs) are estimated to make up the majority of primary PM from road transport, 60% of PM$_{2.5}$ and 73% of PM$_{10}$ in the UK (AQEG, 2019), due to the tightening of EURO exhaust emission requirements.

The key contributors to non-exhaust PM are resuspended road dust and brake, tyre and road surface wear, with minor contributions from

clutch and engine dust (Pant and Harrison, 2013). The estimated contribution of each constituent to non-exhaust PM_{10} varies depending on the sampling location and measurement method (Amato, 2018; Lin et al., 2022; Liu et al., 2022; Matthaios et al., 2022; Harrison et al., 2021; Men et al., 2022; Park et al., 2021; Song et al., 2022). So far, relatively few studies have focused on investigating tyre wear emissions, but have shown that tyre wear particles could contribute up to 11% of total PM_{10} (Baensch-Baltruschat et al., 2020). The latter report tyre wear emission factors for vehicles of different weights on urban roads ranging between 3.8 and 1500 mg/veh.km for motorcycles (TWMV) to heavy duty vehicles (HDV), and Goβmann et al. (2021) report a truck to car tyre wear ratio in environmental samples between 11:1 and 16:1.

In this study, we measured the size-fractionated increase in airborne particle mass across 10 stages of MOUDI impactor samplers located at 2 sites in the UK second largest city, Birmingham. The data were used to estimate brake and tyre wear emission factors using the elemental tracer methodology of Harrison et al. (2012) and the known magnetite concentrations in brake wear (Gonet et al., 2021b). The value of elemental tracers of non-exhaust sources has been confirmed in the work of Grigoratos and Martini (2014) and Charron et al. (2019) and reviewed in Piscitello et al. (2021) and Harrison et al. (2021). The same tracers as used by Harrison et al. (2012) have been applied by Hicks et al. (2021) while using faster response measurement techniques. The use of magnetic properties of particles in this application has not previously been reported. Additionally, in our study, particle size distributions from 10 nm to 10 μm were simultaneously measured at both sites, and the roadside increment data subjected to Positive Matrix Factorisation (PMF) to throw further light on source contributions.

2. Materials and methods

2.1. Birmingham receptor sites

With a population of 1.14 million in 2019 (ONS, 2020), the UK's second largest city, Birmingham, is the focus of our study, conducted at two receptor sites which monitor air quality, namely the Bristol Road Observatory Site (BROS; roadside) and Birmingham Air Quality Site (BAQS; urban background). At these sites (separated by 0.93 km, see Fig. S1). According to the West Midlands road traffic statistics, 4.21 billion vehicle miles were travelled on roads in Birmingham in 2019, of which 3.44 billion were by cars and taxis. PM samples were collected simultaneously over a continuous seven-week period (June 04, 2019–July 23, 2019, Table S2).

2.1.1. Bristol Road Observatory Site (BROS)

The Bristol Road Observatory Site (BROS) (LAT = 52° 26′ 49.711″ N and LONG = 1° 55′ 42.074″ W) is located between two busy traffic-lighted junctions within the University of Birmingham grounds and overlooking the Bristol Road (A38). The first road junction is west of the site, and funnels traffic in and out of Selly Oak, and around the new A38 route passing along the perimeter wall of the University to the New Fosse Way. At the second junction, the dual carriageway of the A38 intersects with a minor road (Bournbrook Road) and the South Gate entrance to the University. At the sampling location, the A38 road runs along a 68° – 248° axis past the site. North of the road is the University campus and south of the site is a dense residential area. The road has an annual average daily flow between the two junctions (referred to as the Aston Webb Boulevard) of 26,027 vehicles per day, consisting of a 97%/3% light duty vehicle (LDV) to HDV mix. This mix can be further disaggregated as: 84.2% cars and taxis; 9.4% LGV; 1.8% rigid HGVs; 0.8% articulated HGVs; 2.2% coaches and buses; and 1.6% TWMV [Bristol Road, Birmingham – Manual Traffic Survey: Tuesday, May 21, 2019, Produced by Streetwise Services Ltd and commissioned by Birmingham City Council]. The road has a 30 mph speed limit and a speed camera after the sampling site on the east-bound carriageway which limits traffic speed.

2.1.2. Birmingham Air Quality Site (BAQS)

The Birmingham Air Quality Site (BAQS) Site (LAT = 52° 27′ 19.872″ N and LONG = 1° 55′ 44.213″ W) was used to quantify the local urban background concentrations. BAQS is one of four air quality supersites in the UK. The Birmingham facility is located within a self-contained cabin in a small green space within the grounds of the University, which itself is surrounded by green space residential and campus facilities. There is a railway line 84 m NW of the site and the nearest roads are: Farquhar Rd (177 m); Edgbaston Park Road (132 m); and Pritchatts Road (262 m). The next largest facility is the Queen Elizabeth Hospital (1.1 km) and the edge of the city centre (taken as the A4540 inner ring-road) is 2.1 km to the NE. Edgbaston Park Road (130 m) carries roughly 4800 vehicles per day and Vincents Drive (316 m) which takes traffic from Pritchatts Road (265 m) and Farquhar Road (178 m) to the Hospital (1 km) carries roughly 6814 vehicle per day (DfT Road Traffic Statistics for counting sites 945,338 and 947,763: https://roadtraffic.dft.gov.uk/local-authorities/141).

2.2. Micro-Orifice Uniform Deposit Impactor (MOUDI)

Our earlier work has shown the value of measurements at roadside and urban background sites for estimating the impacts of road traffic emissions (Gietl et al., 2010; Harrison et al., 2012; Harrison and Beddows, 2017). In this study, we measured the size-fractionated increase in airborne particle mass across 10 stages (Table S2) of MOUDI impactor samplers located at 2 sites in Birmingham.

Described in detail by Marple et al. (1991), the Micro-Orifice Uniform Deposit Impactor (MOUDI) is a cascade impactor which – rather than collecting all suspended PM for typical PMF studies onto a single filter according to whether air is sampled with a $PM_{2.5}$ or PM_{10} inlet – collects size fractions on 10 rotating stages (Table S1). Alternate nozzle and impaction stages rotate distributing the deposited aerosol uniformly around the filter. A total suspended particle (TSP) inlet was used on the MOUDI, and air was sampled at a flow rate of 30 L/min. Each of the 9 upper stages were loaded with PTFE filter substrates and subsequently analysed in the laboratory.

2.3. Laboratory analysis

The main analysis was carried out using Inductively coupled plasma (ICP) – optical emission spectroscopy (-OES) and mass spectroscopy (-MS), supplemented by wavelength dispersive X-ray fluorescence (WD-XRF) and magnetic property measurements. WD-XRF was used to measure Fe, Si and Al concentrations. The magnetic measurements included saturation isothermal remanence magnetisation (SIRM), and anhysteretic remanence magnetisation (ARM), together with magnetic component analysis to quantify concentrations of metallic (zero-valent) Fe and magnetite.

Full details of analytical methods are given in the Supplementary Information.

2.4. Two-step PMF analysis of MOUDI concentration measurements

In air quality work, PMF is routinely applied to time series of data in the form of mass concentration measurements, number concentration size distributions, mass spectrometer ion intensities, to name but a few applications. By the nature of campaign cascade impactor measurements, time series are short in comparison, and in this case, consist of weekly time steps over a campaign of 7 weeks (Table S2). Each weekly measurement consists of 10 filter measurements across the mass size distribution (0.1–40 μm; see Table S1 for size fractions) resulting in 140 fractionated filters, each analysed for elemental concentration, ^mX, and magnetic properties, ^XX. However, in line with the proxy measurements described in Section 3.3, following protocols developed by Harrison et al. (2012), only 4 coarse fractions covering 1.0–9.9 μm were used and we considered only the roadside increment, i.e. the concentration

difference between BROS and BAQS. Furthermore, on closer inspection of the data, Week 3 was not deemed suitable (since a clear roadside increment could not be clearly identified in the data) to be included in the analysis, reducing the dataset down to 24 rows.

Hence the MOUDI input matrix X, comprised 24 rows i of elemental concentration and magnetic properties j, for analysis by PMF using a two-step approach.

In the first step, the elemental concentration data (^mX) was modelled using equation (1) by factors ^mG and ^mF. In order to ensure that the number of explanatory variables was no more than 1/3 of the number of rows of data (recommended for stable PMF), the elements used in the first PMF step were limited to Al, Si, Ca, Cu, Ba, Sn, Fe and Zn. Runs were attempted with a larger number of elements as explanatory variables, but this did not reveal any further insights.

$$^mX = G_1 \bullet F_1 \tag{1}$$

The elemental factors common to all measured stages were represented by matrix ^mF and their contribution to each of the 4 stages for each of the six weeks was given by ^mG. A more detailed description of PMF as applied in this work can be found in Section S4.

In the second step, the matrix G_1 was combined with the magnetic properties ($^{\chi}X$) and subsequently modelled by equation (2).

$$[G_1, ^{\chi}X] = G_2 \bullet ^{\chi}F \tag{2}$$

An fkey matrix was used as a priori information with sufficient pulling strength such that $G_1 = G_2$. A two-step PMF approach was taken with this dataset initially because a successful model could not be achieved using an input matrix combining both the elemental concentrations and magnetic measurements.

2.5. Number size distribution and merging procedure

Particle number size distribution (NSD) data were collected using an SMPS. At BROS, the SMPS comprised a TSI 3080 Electrostatic Classifier with a TSI 3081 DMA and a TSI 3775 CPC and measured from 14.6 to 615 nm using 64 channels per decade. Likewise, at BAQS, the SMPS comprised a TSI 3082 Electrostatic Classifier with a TSI 3081 DMA and a TSI 3750 CPC and measured from 11.8 to 552.3 nm also using 64 channels per decade. Both SMPS were set to collect data over the quarters of the hour. The Coarse NSD data were collected using either Aerodynamic Particle Sizer (TSI 3321 APS) or Optical Particle Counter (TSI 3330 OPC). At BROS the APS collected dN across the size bins 0.523–19.81 μm with a 32 channels per decade and at BAQS the OPC collected dN across a small number of size bins spanning from 0.308 to 8.749 μm with a 12 channels per decade. Both the APS and OPC collected a NSD every 5 min.

With regards to sampling inlets, the APS at BROS sampled at 5 L/min via a vertical 3/8 inch stainless steel sampling tube fitted with a rain cap passing through the cabin roof. The SMPS sampled from a ¼ inch side arm in this vertical inlet at 0.3 L/min. In contrast, at BAQS the SMPS sampled at 1 L/min via a TSI Sampling System for Atmospheric Aerosol (TSI 3772200) and the OPC sampled at 1 L/min through a separate ¼ inch conductive hose.

The NSD measurements were carried out over an 8-week period (Mon June 17, 2019 – Tues Aug 12, 2019). NSD measurements were taken at both roadside and background for the first 5 weeks after which all instruments were run for 3 weeks at the background site for an intercomparison. All data were aggregated to hourly steps.

For both sites these data sets were merged offline onto one common size axis from 14.6 to 10,182 nm using the procedure outlined by Beddows and Harrison (2008). In this procedure, the lower tail of the coarse NSD is fitted to the upper tail of the fine NSD. The coarse NSD is shifted by converting the aerodynamic or optical size data to mobility diameter using a free parameter which is optimised by minimising the separation between the tails of the merged NSD. The free parameter is associated

with the effective density of the particles of diameters within the overlap. The noticeably high noise of the data across the overlap in each merged NSD pair was addressed by fitting a spline. By assigning a relatively low weight in the spline over the overlap and the highest weight to those bins further away from the overlap any measurement error was smoothed out of the data to give a continuous curve without any noticeable kinks in the few data measurements. Finally, the datasets were normalised to the BAQS data using the row of the matrix corresponding to the 2-week intercomparison measurement at the end of the campaign. The remaining 5 weeks from the matrix were then used to create a roadside NSD increment that was analysed using the PMF procedure outlined in the SI.

2.6. Supporting Data

At BROS NO$_x$ was measured using a Thermo Model 42i Chemiluminescence NO–NO$_2$-NO$_x$ Analyzer which was standardised against the Thermo NO$_x$ instrument at BAQS during the intercomparison period. The average measurements for the two sites are given in Table 1, showing typical city values for a UK background and roadside site. At roadside, the NOx, PM$_{10}$ and particle number concentrations were 13.6 μg/m^3, 19.5 μg/m^3 and 7013/cm^3 respectively, all between 30 and 42% higher than the concurrent urban background measurements (Table 1).

Meteorological data used in this study (wind direction and wind speed) were collected from Birmingham Airport (LAT = 52° 27′ 10.080″ N and LONG = 1° 44′ 32.820″ W) which is considered to be representative of the conditions over Birmingham as a whole (Met Office, 2019). The average temperature and pressure were 16 °C and 1016 mbar, respectively (Table 1). The rainfall over the sampling periods is given in Table S2. The weekly rainfall was highest during week 1 and 2. It was notably wetter in those weeks, and the third, when the total rainfall was just higher than the yearly average value. These three weeks were also accompanied by the highest maximum hourly average between 14 and 16 mm/h corresponding to very heavy rain. Weeks 4, 5 and 6 were the driest sampling periods and hence more conducive to the resuspension of road dust.

2.7. PMF analysis of NSD measurements

A similar approach to the PMF analysis of the MOUDI data was carried out on the NSD data whereby the roadside increment was factorised. In contrast to the MOUDI PMF analysis, the hourly time series were entered as matrix X in equation (3) giving us the capacity to understand the diurnal behaviour of the sources and link them to meteorological data presented in bivariate plots (Fig. S7). Details of the analysis are presented in the supporting information.

$$^{nsdincrement}_{hourly}X = _{hourly}G \bullet F_{source\ increment} \tag{3}$$

Table 1

Average measurements at the Birmingham sites from June 04, 2019 to July 23, 2019 (mean ± stdev). A Wilcoxon test showed that the difference (for all: NOx, NOx, PM$_{2.5}$, PM$_{10}$, PN) was significant (p < 0.0001, effect size r = 0.3).

Measurement	BAQS	BROS
NO$_x$ [μg/m^3]	9.8 ± 11	14 ± 10
PM$_{2.5}$ [μg/m^3] FIDAS	8.6 ± 5.7	11 ± 7.5[a]
PM$_{10}$ [μg/m^3] FIDAS	15 ± 8	20 ± 11*
Number Concentration [1/cm^3]	4950 ± 3240	7010 ± 3920
Temperature [ºC] Elmdon	16 ± 4.1	–
Pressure [mbar] Elmdon	1016 ± 7	–

[a] Values measured using the merged volume size distribution measured using a TSI SMPS and APS pair and an estimated particle density of 1.3 g/cm^3, also indicated by the FIDAS measurements. Klockner et al. (2021) reported the density of TRWPs was mostly in the range of 1.3–1.7 g/cm^3.

3. Results

The results of the laboratory analyses and the processing of the data are presented in the following sections starting with the laboratory measurements.

3.1. Description of the size-fractionated elemental and magnetic measurements

The size-fractionated measurements for the two sites are presented in Fig. 1 and the full suite of metals is plotted for all MOUDI stages in Figs. S4 and S5. From this, the roadside and regional background contributions can be readily distinguished. For example, the mass distributions of Na and Mg, likely to be predominantly from a marine source, are as expected almost the same for both sites, since a background marine source would impact both BROS and BAQS to the same extent. Conversely, there are clear roadside increments for Fe and the magnetic metrics (SIRM, magnetite, and zero-valent Fe) which are expected to be associated with brake dust (Gonet et al., 2021a), although resuspension of road dust can also contribute to the Fe (Piscitello et al., 2021). Ba and Cu, widely used tracers of brake dust are also elevated at the roadside.

Al, Ca, Si and Ti, crustal elements associated with resuspension, show a roadside increment, as does Zn, widely taken as a tracer of tyre wear (Harrison et al., 2021).

At the roadside, SIRM values (representing the content of ferrimagnetic, remanence-bearing particles) and metallic Fe (zero-valent Fe) concentrations were highest for particles ~ 5–8 μm in nominal diameter (many such particles occur as agglomerations of much smaller, nanoscale particles; Gonet et al., 2021b). Magnetite concentrations were highest for particles >10 μm, with a smaller peak evident for particles ~2.5 μm. For all particles >1 μm in size, increments at the roadside (compared to background values) are observed for all of the magnetic particle metrics; i.e., for SIRM (86% higher than background), ARM (representing ferrimagnetic particles ~ 0.03 μm in size, 47%), magnetite content (76%), and zero-valent Fe (undetectable at the BAQS site). Notable is that the roadside magnetite content and SIRM vary with PM size in a similar fashion as previously observed for experimental, dynamometer-derived brake-wear PM (Gonet et al., 2021b); i.e., with peaks for particles >10 μm and ~ 5 μm. This consistency is unsurprising given that the SIRM-carriers for roadside PM are often dominated by brake-derived particles in urban environments. Indeed, specifically at this roadside site (BROS), ~ 79–91% of airborne magnetite particles

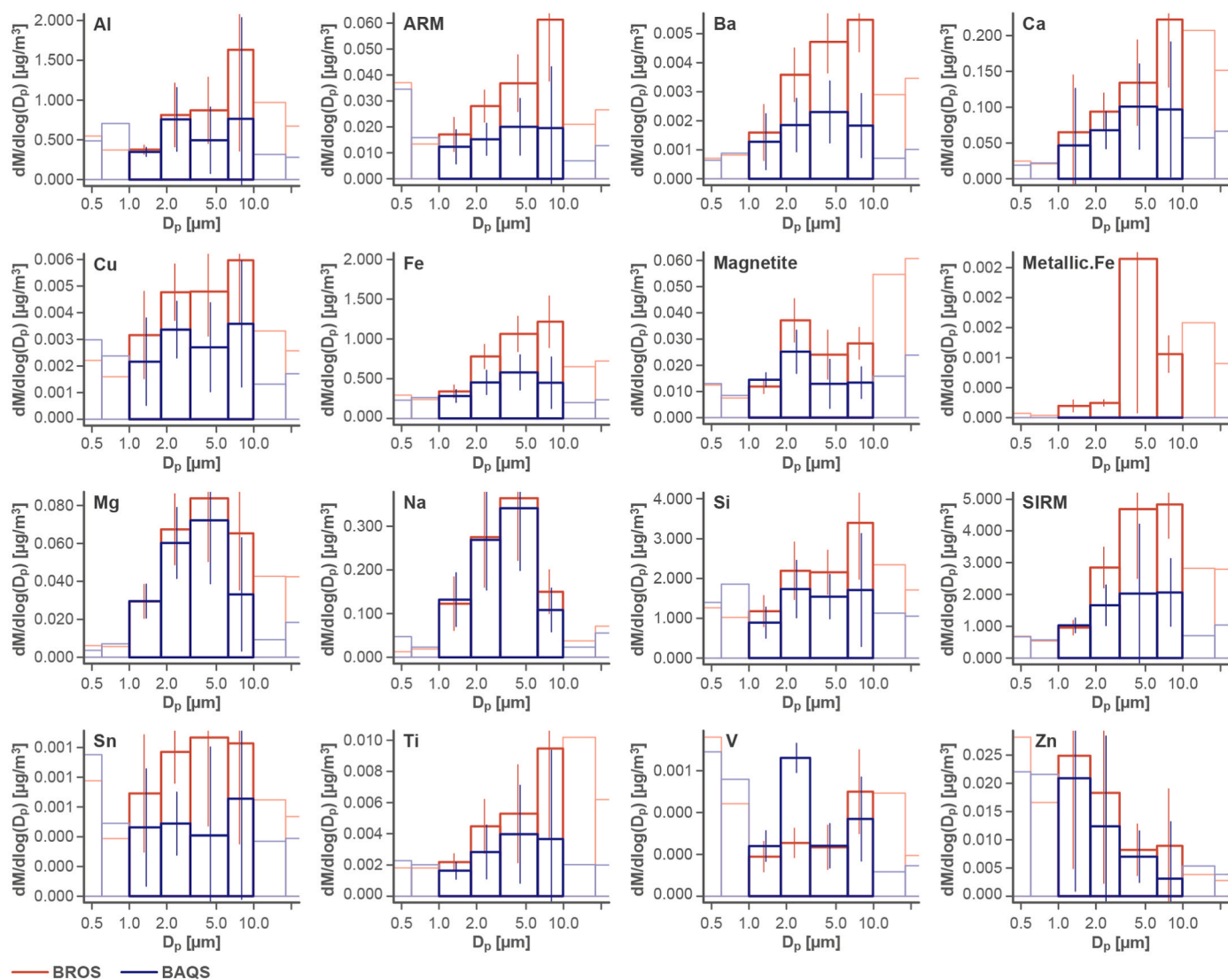**Fig. 1.** Size fractionated elemental concentrations measured from the MOUDI stages at BAQS and BROS. [Red and blue bars show contribution at BROS and BAQS respectively; darker red and blue indicate which measurements were used in the PMF and proxy apportionment calculations.]. (For interpretation of the references to colour in this figure legend, the reader is referred to the Web version of this article.)

originated from vehicle brake systems, as shown in our previous study (Gonet et al., 2021a). The observation of zero-valent Fe at the roadside probably reflects the sampling of fresh wear particles from the brake discs, which rapidly oxidise on mixing with ambient air.

3.2. Evaluation of sources

3.2.1. Sources identified from the elemental data using MOUDI PMF

The application of PMF to the roadside increment elemental concentrations identified 3 sources which were associated with brake dust, tyre dust and crustal material (normally resuspension). When Si was included in the input matrix, an extra crustal factor was required to balance the model. This resulted in a 4-factor solution with 2 crustal factors with high and low Si concentrations, respectively. The profiles of the Si-free model consisted of 3 factors, for which G and F are presented in Fig. 2 and S6, respectively. The F matrix represents the roadside increment in elemental and magnetic metrics of the factors, and G represents the overall increment which those factors contribute to the 4 MOUDI stages each week. The explained variations EV_f are included in Fig. 2 whereas EV_g is plotted separately as Fig. S6. Note that for Fig. 2 and S6, the weekly size distribution is given as line graphs but the overall average campaign size distribution for each factor is included as a bar chart, the widths of each bar representing the width of the size bin represented by the MOUDI impactor stage. The explained variation helps determine how an elemental concentration or magnetic metric contributes to each factor and is often more useful than the increment

given in F which often needs a log scale (not used here since F is treated as secondary to EV_f) for all concentrations to be shown.

Considering each source in turn, the brake dust factor is identified by its strong contribution to Ba and Fe, together with contributions to Cu and Sn. These elements are expected to be predominantly emitted by brake wear, while Zn is primarily due to tyre wear and to a lesser degree from brake wear (Budai and Clement, 2018; Harrison et al., 2021; Fussell et al., 2022). For a coarse brake wear factor, magnetite (Fe_3O_4), wustite (FeO), haematite (Fe_2O_3), Cu oxides, Sb (III), Sb (V), Sn, Ba, Zr and Al can be expected to be present (Gonet et al., 2021b; Mulani et al., 2022). This factor has a mass modal diameter from 3.1 to 6.2 μm, consistent with values reported previously for brake wear (Harrison et al., 2021; Gonet et al., 2021b). This characterisation is further supported by the second step PMF analysis which shows that the brake dust factor has the highest contribution of all the factors to SIRM, zero-valent Fe, and magnetite, with a lesser contribution from the crustal (resuspension) factor.

Brake-wear PM emissions are very strongly magnetic compared to other types of emissions in roadside environments (Gonet and Maher, 2019; Gonet et al., 2021b), displaying high SIRM and magnetite contents (e.g., 100–1000 × higher than exhaust emissions), and also comprise one of the very few sources of metallic (zero-valent) Fe in roadside PM (Gonet et al., 2021b). Here, factor 3 contributes most to SIRM, zero-valent Fe and magnetite as indicated by the values of Explained Variation between 0.24 and 0.42. Given that SIRM for brake-wear PM is ~ 300 higher than that of crustal PM in Birmingham (Gonet et al.,
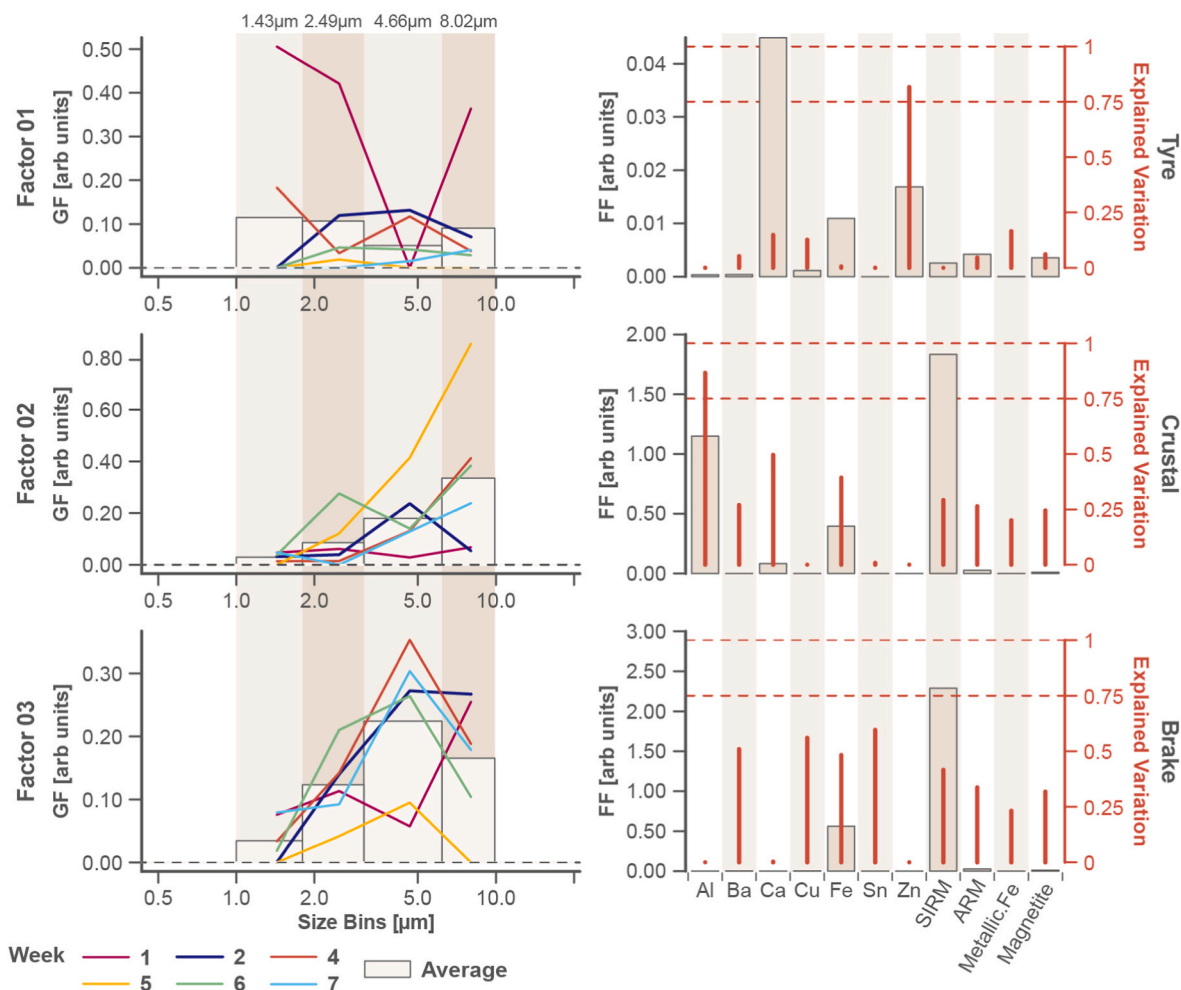

Fig. 2. Metal and Magnetic factors: left Size resolved components reconstructed from matrix G; right concentration profiles, matrix F and (b) explained variation matrix EV_f. Roadside increment of the factors 1–4 calculated from the G Matrix. [The equivalent plots for the explained variation EV_g are given in Fig. S3.].

2021a, 2021b), it is unsurprising that factor 3 (brake wear) explains a similar or greater portion of the magnetic metric variation compared to factor 2 (crustal/construction), even though the factor 2-related emission factor, EF is more than an order of magnitude higher than that for factor 3 (brakes) (Table 2). It is also evident that the magnetic metrics are strongly or moderately correlated with typical brake-wear elemental tracers; SIRM values are directly correlated with Ba (n = 70; R = 0.74), Cu (n = 70; R = 0.67), and Fe (n = 70; R = 0.88) content, and magnetite with Ba (n = 70; R = 0.62), Cu (n = 70; R = 0.51), and Fe (n = 70; R = 0.64). In addition, it is also worth pointing out that the crustal factor also explains a large fraction of Fe, SIRM, ARM, metallic Fe and magnetite which is likely unnaturally elevated due to mixing of road dust.

Based on our magnetic component analysis (see S5) and the assumption that brake-wear constitutes $\sim$ 83% of the total airborne magnetite particles at BROS (Gonet et al., 2021a), we estimate that brake-wear constitutes an increase (Δ), $\Delta PM^{mag}_{1.0-9.9} = 0.116 \ \mu g/m^3$ (particles between 0.9 μm and 9.9 μm).

In contrast, the tyre dust factor makes a small contribution to magnetic properties (unsurprisingly, since this a priori information was included in the model) but makes a strong contribution to Zn, with a bimodal size distribution with modes between 0.6 and 1.0 μm (excluded from the analysis) and 6.2 and 9.9 μm. In published work, Oroumiyeh and Zhu (2021) measured at-wheel brake particles as a unimodal mass size distribution with a mode diameter of 3–4 μm, whereas their at-tyre measurements showed particles with a slightly larger mode diameter of 4–5 μm. However, Kreider et al. (2010) found a distribution with a much greater modal diameter (50–80 μm). The measured distribution is likely to be determined predominantly not by the emission, but by the atmospheric transport and deposition properties of the particles and the inlet characteristics of the sampler. The sub-micrometre mode may be due to exhaust emissions of zinc arising from combustion of zinc-based oil additives (Harrison et al., 2003), but may also arise from tyre wear.

The crustal factor is identified from the elevated Al and Ca values. Again, it is accompanied by trace elements and magnetic metrics associated with brake wear (Ba, Fe, SIRM, ARM, zero-valent Fe and magnetite). Such roadside dust is deposited on the road surface and mixed with the crustal material deriving from roadside soil and mineral material used in the road surface. The modal diameters are also clearly well above 10 μm, characteristic of suspended dust.

3.2.2. Sources identified using NSD PMF

The hourly roadside incremental NSD data (10 nm–10 μm) were analysed using PMF according to the description given in S4.2. Four factors – using both the number and volume size distributions calculated from the F matrix - were identified as most appropriately representing the sources associated with the roadside increment. Factor splitting was clearly observed in the 6-factor solution, and 5 factors did not provide a satisfactory resolution. Considering Fig. 3, factors A and C are clearly most prominent in the number size distribution and show diurnal trends in matrix G which are characteristic of hourly traffic counts. These factors are attributed to exhaust emissions, the first being due to nucleation mode particles, with the second due to the larger solid carbon particles. With number modal diameters of around 25 nm and 70 nm, respectively, these factor assignments are very consistent with their

identification in earlier studies (Rivas et al., 2020; Dai et al., 2021; Tremper et al., 2022; Wu et al., 2021). In contrast, factors B and D make an insignificant contribution to the number size distribution but when plotted as volume, it is clear that factor B is from a coarse material and factor D, with a mode in the volume distribution at around 500 nm, and a nocturnal predominance is from an unexpected, and unidentified source, possibly biomass burning from the residential area bordering the A38 road. The crustal factor (factor B) shows a strong daily diurnal trend peaking at midday, whereas factor D is strongest during the evening, through the night and declines during the day. Fig. S7 presents the polar plots of G for the 4 NSD-Factors. It is evident that factor D is a local source, diluted as the wind speed increases and has a morning component from the direction of the road (SSW of the BROS site). The crustal factor (factor B) is elevated at midday for winds west of the site, in particular between 247 and 270°. The solid exhaust factor (factor C) shows an association particularly with wind directions from the east along the Bristol Road, most notably its division into two highways after a complex traffic lighted junction. Factor A shows a much more complex association with wind direction (Fig. S7), and a strong tendency to peak in the middle of the day. This is strongly suggestive of inclusion of events of particle nucleation which can create larger numbers of particles and higher growth rates at roadside than nearby urban background sites (Bousiotis et al., 2021)

3.3. Emission factors derived from elemental proxies, PMF factors and magnetic measurements

In this work, we used 2 different methods to estimate the emission factors for brake and tyre wear: (1) an elemental tracer proxy method and (2) the PMF-based method. Additionally, we estimated the emission factor for brake wear using a 3rd method, i.e., based on magnetic metrics (Table 2).

For the tracer proxy approach, the emission factors from brake and tyre wear are estimated from concentrations of tracer elements together with an estimate of the dilution in roadside air. In this work, Ba, Zn and Si are used as tracers of brake and tyre wear and resuspension respectively, and the methodology reported by Harrison et al. (2012) is used to estimate a roadside incremental concentration. Table 2 shows the mass concentration increments and emission factors calculated using the roadside increments of Ba, Si and Zn. For each concentration increment, summed over the stages covering the aerodynamic diameter >1.0 μm, a scaling factor and dilution factor were applied. It is assumed that 50% of the measured Zn in the super micrometre particles arises from tyre wear, and the Zn content of tyre rubber is 1%, and hence a factor of 50 is applied to the roadside Zn increment. In the case of brake dust, the Ba roadside increment has been scaled by a factor of 91, based on the estimate that Ba represented about 1.1% of the mass of brake dust particles (Gietl et al., 2010; Harrison et al., 2012). Similarly, given the fact that Si represents 27.7% of average earth crustal material, the Si roadside increment was scaled by a factor of 3.6 in order to represent the mass of resuspended particles.

In addition to the tracer proxy method, an increment was also calculated using the PMF factors. From the PMF analysis, the data from the stages, X, were resolved into G and F, whereby F are the composition profiles and G are the contributions of those profiles to the stages in the

Table 2

Particulate Mass emission factors calculated using (a) the Tracer Proxy methodology described by Harrison et al. (2012) and (b) the VSD increment modelled by PMF. [For conversion from ΔPN and ΔPM to EF see S3.3, using a Dilution Factor = 0.018 $\mu g/m^3 (g/km)^{-1}$ and traffic flow of 1383 veh/hr.] For the magnetic size measurements $\Delta PM^{mag}_{1.0-9.9} = 0.116 \ \mu g/m^3$, the brake emission factor derived from the magnetic size measurements $EF^{mag}_{1.0-9.9} = 4.69$ mg/veh.km.

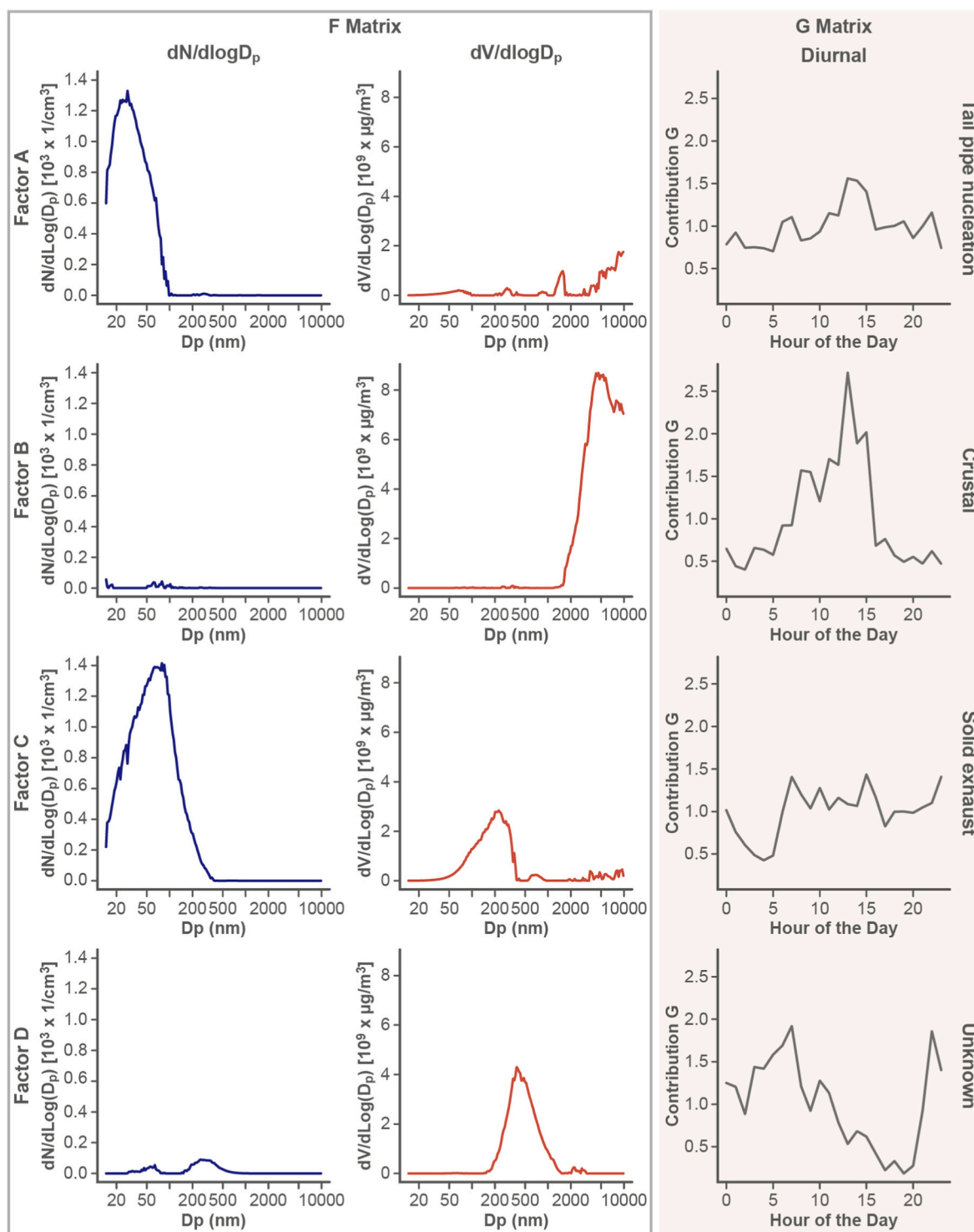| Source	Proxy	Tracer Proxy		PMF Factor Derived		EMEP/EEA Estimate
		$\Delta PM^{t-p}_{1.0-9.9}$	EF^{t-p}	$\Delta PM^{PMF}_{1.0-9.9}$	EF^{PMF}	$EF^{EMEP/EEA}$
		$\mu g/m^3$	mg/veh.km	$\mu g/m^3$	mg/veh.km	mg/veh.km
Brake	[Ba] x 91	0.182	7.38	0.109	4.41	3.4
Tyre	[Zn] x 50	0.245	9.92	0.268	10.9	2.5

Fig. 3. Four factor NSD-PMF solution: left F - expressed as number size distributions, NSD; middle F - expressed volume distributions (VSD) and right G - expressed as the average diurnal trend.

MOUDI. The model calculates a G value for each stage of the MOUDI and for each factor which is then tabulated against a PM value for the stage calculated from the NSD data (see S4.4). The PM value is regressed against the G values and used to assign a quantified mass increment to the stages. Using this approach, we do not lose any of the mass accounted for in the laboratory analyses by the exclusion of metal concentrations from the matrix. The metals, Ba, Cu, Fe, Zn, Ca and Al are used in the model to identify brake, tyre and crustal factors through matrix F and the 'calibrated' G values are used to apportion all of the

expected mass associated with those factors.

As summarised in Table 2, the tracer-proxy $\Delta PM_{1.0-9.9}^{t-p}$, factor-derived $\Delta PM_{1.0-9.9}^{PMF}$ and magnetically-derived $\Delta PM_{1.0-9.9}^{mag}$ roadside concentration increments are all comparable for brake and tyre wear. The brake wear $^{br}\Delta PM_{1.0-9.9}^{t-p}$, $^{br}\Delta PM_{1.0-9.9}^{PMF}$ and $^{br}\Delta PM_{1.0-9.9}^{mag}$ increment estimates were 0.18, 0.11 and 0.12 µg/m³ respectively, and the tyre wear increments $^{ty}\Delta PM_{1.0-9.9}^{t-p}$ and $^{ty}\Delta PM_{1.0-9.9}^{PMF}$ were 0.25 and 0.27 µg/m³. In comparison, the estimated increment for resuspension $^{crust}\Delta PM_{1.0-9.9}^{t-p}$

and $^{crust}\Delta PM_{1.0-9.9}^{PMF}$ display huge values of 2.1 and 3.5 µg/m^3, respectively. These values were then converted (below) to emission factors using traffic count estimates and NO$_x$ concentrations.

Extensive traffic data were not measured during the campaign and instead traffic surveys were relied on to calculate the dilution factor. For a typical 24-h diurnal cycle, 24 pairs of measured roadside NO$_x$ increment were regressed against the fleet emission of NO$_x$ estimated using emission factors derived from the. UK National Atmospheric Emissions Inventory (NAEI. UK, 2019). The emissions of NO$_x$ were summed from cars, LDV, Rigid, Articulated, Bus/Coach, and TWMV weighted by counts collected by a daytime junction survey carried out manually by Birmingham City Council (May 21, 2019). The NO$_x$ emission data were scaled for each hour of a diurnal cycle by a total traffic count to give an hourly emission. Using the methodology of the 2019 European Monitoring and Evaluation Programme/European Environment Agency (EMEP/EEA) Guidebook (EMEP/EEA, 2019), emissions from brake and tyre wear from the vehicle fleet were also estimated. For PM$_{10}$, total emissions from conventional passenger vehicles range from 5 to 16 mg/km, but these vary hugely as a function of weight and consequently the fleet composition (see discussion below). For our case study, Bristol Road at the University of Birmingham, the PM$_{10}$ brake and tyre dust were estimated from the vehicle fleet passing the site to be 3.4 and 2.5 mg/veh.km, respectively.

On average, a traffic flow of 1383 vehicles per hour passed the junction adjacent to the BROS site and an average dilution factor 0.018 µg/m^3(g/km)$^{-1}$ was estimated using the calculations given in S4.3 and presented in Table 2 alongside the calculated increments. Using the tracer proxy method described above, the increments ΔPM above yielded brake dust EF_{br}^{t-p} and tyre dust EF_{ty}^{t-p} emission factor of 7.4 and 9.9 mg/veh.km respectively, which may be compared with values estimated from the EMEP/EEA Guidebook (EMEP/EEA, 2019) of $EF_{br}^{EMEP/EEA} = 3.4$ and $EF_{ty}^{EMEP/EEA} = 2.5$ mg/veh.km). Furthermore, given a roadside increment of $\Delta PM_{1.0-9.9}^{mag} = 0.116$ µg/m^3, the brake emission factor derived from the magnetic measurements $EF_{br}^{mag} = 4.69$ mg/veh.km. A similar calculation was carried out using the apportioned increment in mass calculated for each PMF factor (see section S4.3), yielding a PM$_{10}$ brake dust EF_{br}^{PMF} and tyre dust EF_{ty}^{PMF} emission factor of 4.4 and 11 mg/veh.km, respectively (Farwick zum Hagen et al., 2019).

The crustal calculations, typically treated as resuspension, yielded a consistently high value of $EF_{crust}^{t-p} = 86$ mg/veh.km and $EF_{crust}^{PMF} = 143$ mg/veh.km. The polar plot of this factor shown in Fig. S7 strongly indicated that its source was predominantly from a large neighbouring construction site (see Fig. S8). Elevated wind speeds between 247 and 270° correspond both to the increase in this crustal NSD-Factor and the direction of an ongoing development centred at the Battery Park. It therefore seems likely that the roadside increment and resuspension emission factor at this roadside site are at present largely unrelated to road traffic. Factor 2 from the NSD data analysis was notable in that its roadside increment (3.5 µg/m^3) was of a similar magnitude to that derived for the crustal factor measured using the MOUDI (3.2 µg/m^3).

4. Discussion

In this work, we measured the increment in elemental mass concentrations and magnetic properties measured from filter samples collected on the size-fractionated impactor stages of two MOUDI impactors co-located at a roadside and background site at the University of Birmingham during the spring/summer of 2019. For the PMF analysis, rather than the traditional approach of analysing the time series – which for the MOUDI would restrict our dataset to 6 measurements – we analysed the mass concentrations across each of 4 of the 10 impactor stages (1.0–9.9 µm) for the 6 of the best 7 weekly samples using PMF. This resulted in the identification of sources which impacted all the stages but to different degrees according to the size range. Further, the

PMF analysis was extended with a second step which fitted the G matrices from the first step to the measured PM magnetic properties.

Since it is the roadside increment which is analysed by PMF, regional sources are not expected to be identified since these contribute equally at both background and roadside. However, these results demonstrate that the roadside site and its increment were heavily impacted by a local construction site, elevating the contribution of the crustal factor to 83% of the mass, c.f. brake dust (7.1%) and tyre dust (9.6%). In an ideal situation, our third factor ought to account for the vehicle resuspension at the roadside site (BROS). However, accompanying hourly merged SMPS-APS data collected at the site help elucidate this outlier. Meteorological data plotted against the time series of the PMF factors derived from the merged data showed a wind directional dependence on a large commercial construction site 1–2 km WSW of the site. Interestingly, the estimated roadside increment of this NSD-PMF derived factor was 3.2 µg/m^3 which is in line with a MOUDI-PMF derived value in this work of $^{crust}\Delta PM_{1.0-9.9}^{PMF} = 3.5$ µg/m^3 (c.f. a lower tracer-proxy value of $^{crust}\Delta PM_{1.0-9.9}^{t-p} = 2.1$ µg/m^3). Hence, rather than refer to resuspension, we have named this source 'crustal' to account for the large contribution from the construction site.

Using Ba and magnetic metrics as tracers, the brake wear emission factor was estimated as $EF_{br}^{t-p} = 7.4$ mg/veh.km and $EF_{br}^{mag} = 4.7$ mg/veh.km. The tyre wear emission factor (tracer proxy method; Zn as tracer) was $EF_{ty}^{t-p} = 9.9$ mg/veh.km. In comparison, PMF-based emission factors are $EF_{br}^{PMF} = 4.4$ mg/veh.km (for brake wear) and $EF_{ty}^{PMF} = 10.9$ mg/veh.km (for tyre wear) (Table 2). These values are very close or exceed the regulated exhaust emission limit of 4.5 mg/veh.km (Euro 6 limit for LDVs), and the upcoming Euro 7 limit for brake wear-derived PM$_{10}$ of 7 mg/veh.km, to be implemented in 2 years' time. Farwick zum Hagen et al. (2019) investigated brake wear emissions during on-road driving with a midsize passenger car on a closed test track. A novel sampling system was designed that aimed at monitoring the entire aspiration of brake wear particles in the Los Angeles City Traffic (LACT) cycle, representative of realistic driving behaviour. For two different brake materials, PM$_{10}$ emission factors ranged from $^{br}EF_{10} = 5.6$ mg/veh.km to 8.4 mg/veh.km. For tyre wear, Grigoratos and Martini (2014) present an average value of $^{ty}EF_{10} = 6.3$ mg/veh.km. Higher brake and tyre dust emissions might be expected at BROS due to the higher loads caused by braking into and accelerating out of a traffic lighted junction as brake dust emissions can vary depending on braking conditions as well as measurement protocol (Hagino et al., 2015).

The respective fleet exhaust number emission factors were $EF_{exh\_nucl}^{PMF} = 1.9 \times 10^{12}$/veh.km and $EF_{exh\_core}^{PMF}$ 2.8×10^{12}/veh.km. Taking the sum of the emission factors, a composite emission factor of 4.7×10^{12}/veh.km for the typical vehicle fleet passing BROS, 86% of which are passenger cars. This EF significantly exceeds the Euro-6/7 limit for exhaust particle number (both Euro-6 and Euro-7 limits for non-volatile particle number $= 6 \times 10^{11}$/veh.km). Based on a survey of recent measurements, 4.7×10^{12}/veh.km is in the vicinity of laboratory and field values for a general UK fleet 0.53:0.47 split between petrol and diesel vehicles [2019 ratio calculated from table VEH1103 from https://www.gov.uk/government/statistical-data-sets/vehicle-licensing-statistics-data-tables]. Boveroux et al. (2021) looked at the impact of mileage on particle number emission factor distributions for EURO 5 and 6 diesel European passenger cars based on the measurements of 757 vehicles, reporting emission factors in the region of 0.60–5.8 $\times 10^{12}$/veh.km. These are in line with earlier studies carried out by Momenimovahed et al. (2015) who measured Canadian passenger cars with model years 2012–2014. The number emission factors (for particles larger than 2.5 nm) ranged between 0.55 x 10^{12} and 3.50 x 10^{12}/veh.km for freshly emitted (nascent) particles and between 0.29 x 10^{12} and 3.31 x 10^{12}/veh.km for non-volatile (thermodenuded) particles.

5. Conclusions

In summary, here we used three different methods (tracer proxy, PMF and magnetic measurements), combined with particle size distribution data, to estimate emission factors for brake and tyre wear at a roadside site in Birmingham, UK. They give broadly consistent results. Brake wear emission factors ranged between 4.4 and 7.4 mg/veh.km, and tyre wear between 9.9 and 10.9 mg/veh.km. A third factor was identified related to crustal emissions from a nearby construction site, and was so large as to obscure resuspension emissions from the highway. Additionally, exhaust number emission factors at the site were estimated at 1.9×10^{12}/veh.km for nucleation mode particles and 2.8×10^{12}/veh. km for solid carbon particles. Given the current shift towards battery-electric vehicles, the measurement and modelling of non-exhaust emissions will become of increasing importance.

Funding

Declaration of competing interest

The authors declare that they have no known competing financial interests or personal relationships that could have appeared to influence the work reported in this paper.

Data availability

Data supporting this publication are openly available from the UBIRA eData repository at https://doi.org/10.25500/edata. bham.00000745.

Appendix A. Supplementary data

Supplementary data to this article can be found online at https://doi. org/10.1016/j.envpol.2023.121830.

References

Amato, F., 2018. In: Amato, F. (Ed.), Non-Exhaust Emissions. An Urban Air Quality Problem for Public Health Impact and Mitigation Measures. Academic Press. https:// doi.org/10.1016/B978-0-12-811770-5.01001-3. (Accessed 28 September 2022) [Last accessed.

AQEG, 2019. Non-exhaust Emissions from Road Traffic. Air Quality Expert Group, Department for Environment Food and Rural Affairs, London. https://uk-air.defra.go v.uk/assets/documents/reports/cat09/1907101151_20190709_Non_Exhaust_Emiss ions_typeset_Final.pdf. (Accessed 28 September 2022) [Last accessed.

Baensch-Baltruschat, B., Kocher, B., Stock, F., Reifferscheid, G., 2020. Tyre and road wear particles (TRWP) - a review of generation, properties, emissions, human health risk, ecotoxicity, and fate in the environment. Sci. Total Environ. 733, 137823.

Beddows, D.C.S., Harrison, R.M., 2008. Comparison of average particle number emission factors for heavy and light duty vehicles derived from rolling chassis dynamometer and field studies. Atmos. Environ. 42, 7954–7966.

Bousiotis, D., Pope, F., Beddows, D., Dall'Osto, M., Massling, A., Klenø Nøjgaard, J., Nordstrøm, C., Niemi, J.V., Portin, H., Petäjä, T., Perez, N., Alastuey, A., Querol, X., Kouvarakis, G., Mihalopoulos, N., Vratolis, S., Eleftheriadis, K., Wiedensohler, A., Weinhold, K., Merkel, M., Touch, T., Harrison, R.M., 2021. A phenomenology of new particle formation (NPF) at 13 European sites. Atmos. Chem. Phys. 21, 11905–11925.

Boveroux, F., Cassiers, S., De Meyer, P., Buekenhoudt, P., Bergmans, B., Idczak, F., Jeanmart, H., Verhelst, S., Contino, F., 2021. Impact of mileage on particle number emission factors for EURO5 and EURO6 diesel passenger cars. Atmos. Environ. 244, 117975.

Budai, P., Clement, A., 2018. Spatial distribution patterns of four traffic-emitted heavy metals in urban road dust and the resuspension of brake-emitted particles: findings of a field study. Transplant. Res. Part D 62, 179–185.

Charron, A., Polo-Rehn, L., Besombes, J.-L., Golly, B., Buisson, C., Chanut, H., Marchand, N., Guillaud, G., Jaffrezo, J.-L., 2019. Identification and quantification of particulate tracers of exhaust and non-exhaust vehicle emissions. Atmos. Chem. Phys. 19, 5187–5207.

Dai, Q., Ding, J., Song, C., Liu, B., Bi, X., Wu, J., Zhang, Y., Feng, Y., Hopke, P.K., 2021. Changes in source contributions to particle number concentrations after the COVID-19 outbreak: insights from a dispersion normalized PMF. Sci. Total Environ. 759, 143548.

Dataset, O.N.S., 2020. Analysis of Population Estimate Tool [last accessed 28th of September 2022. Office for National Statistics. https://www.ons.gov.uk/peopl epopulationandcommunity/populationandmigration/populationestimates/dataset s/analysisofpopulationestimatestool.

EMEP/EEA, 2019. EMEP/EEA air pollutant emission inventory guidebook. Technical guidance to prepare national emission inventories. European Environment Agency EEA Report No 13/2019, ISSN 1977-8449, Section 1.A.3.b.vi, Road transport: Automobile tyre and brake wear, https://www.eea.europa.eu/publications/eme p-eea-guidebook-2019/download. (Accessed 21 May 2023) [Last accessed].

Farwick zum Hagen, F.H., Mathissen, M., Grabiec, T., Hennicke, T., Rettig, M., Grochowicz, J., Vogt, R., Benter, T., 2019. On-road vehicle measurements of brake wear particle emissions. Atmos. Environ. 217, 116943.

Fussell, J.C., Franklin, M., Green, D.C., Gustafsson, M., Harrison, R.M., Hicks, W., Kelly, F.J., Kishta, F., Miller, M.R., Mudway, I.S., Oroumiyeh, F., Selley, L., Wang, M., Zhu, Y., 2022. A review of road traffic-derived non-exhaust particles: emissions, physicochemical characteristics, health risks, and mitigation measures. Environ. Sci. Technol. 56, 6813–6835.

Gietl, J.K., Lawrence, R., Thorpe, A.J., Harrison, R.M., 2010. Identification of brake wear particles and derivation of a quantitative tracer for brake dust at a major road. Atmos. Environ. 44, 141–146.

Gonet, T., Maher, B.A., 2019. Airborne, vehicle-derived fe-bearing nanoparticles in the urban environment: a review. Environ. Sci. Technol. 53, 9970–9991.

Gonet, T., Maher, B.A., Kukutschová, J., 2021a. Source apportionment of magnetite particles in roadside airborne particulate matter. Sci. Total Environ. 752, 141828.

Gonet, T., Maher, B.A., Nyirő-Kósa, I., Pósfai, M., Vaculík, M., Kukutschová, J., 2021b. Size-resolved, quantitative evaluation of the magnetic mineralogy of airborne brake-wear particulate emissions. Environ. Pollut. 288, 117808.

Goßmann, I., Halbach, M., Scholz-Böttcher, B.M., 2021. Car and truck tire wear particles in complex environmental samples – a quantitative comparison with "traditional" microplastic polymer mass loads. Sci. Total Environ. 773, 145667.

Grigoratos, T., Martini, G., 2014. Non-exhaust traffic related emissions. Brake and tyre wear PM. JRC Science and Policy Reports. Rep. Eur. 26648, 7–9. https://publication s.jrc.ec.europa.eu/repository/bitstream/JRC89231/jrc89231-online%20final% 20version%202.pdf. (Accessed 23 January 2023) [Last accessed.

Hagino, H., Oyama, M., Sasaki, S., 2015. Airborne brake wear particle emission due to braking and accelerating. Wear 334–335, 44–48.

Harrison, R.M., Beddows, D.C., 2017. Efficacy of recent emissions controls on road vehicles in Europe and implications for public health. Sci. Rep. 7, 1152.

Harrison, R.M., Tilling, R., Callen Romero, M.S., Harrad, S., Jarvis, K., 2003. A study of trace metals and polycyclic aromatic hydrocarbons in the roadside environment. Atmos. Environ. 37, 2391–2402.

Harrison, R., Jones, M., A, M., Gietl, J., Yin, J., Green, D.C., 2012. Estimation of the contributions of brake dust, tire wear and resuspension to nonexhaust traffic particles derived from atmospheric measurements. Environ. Sci. Technol. 46, 6523–6529.

Harrison, R.M., Allan, J.D., Heald, M.R., Lewis, A.C., Marner, B., Murrells, T., Williams, A., 2021. Non-exhaust vehicle emissions of particulate matter and VOC from road traffic: a review. Atmos. Environ. 262, 118592.

Hicks, W., Beevers, S., Tremper, A.H., Stewart, G., Priestman, M., Kelly, F.J., Lanoisellé, M., Lowry, D., Green, D.C., 2021. Quantification of non-exhaust particulate matter traffic emissions and the impact of COVID-19 lockdown at London Marylebone Road. Atmosphere 12, 190.

Klockner, P., Seiwert, B., Weyrauch, S., Escher, B.I., Reemtsma, T., Wagner, S., 2021. Comprehensive characterization of tire and road wear particles in highway tunnel road dust by use of size and density fractionation. Chemosphere 279, 130530.

Kreider, M.L., Panko, J.M., McAtee, B.L., Sweet, L.I., Finley, B.L., 2010. Physical and chemical characterization of tire-related particles: comparison of particles generated using different methodologies. Sci. Total Environ. 408, 652–659.

Lin, Si, Liu, Y., Chen, H., Wu, S., Michalaki, W., Proctor, P., Rowley, G., 2022. Impact of change in traffic flow on vehicle non-exhaust PM2.5 and PM10 emissions: a case study of the M25 motorway, UK. Chemosphere 303, 135069.

Liu, Y., Chen, H., Li, Y., Gao, J., Dave, K., Chen, J., Li, T., Tu, R., 2022. Exhaust and non-exhaust emissions from conventional and electric vehicles: a comparison of monetary impact values. J. Clean. Prod. 331, 129965.

Marple, V.A., Rubow, K., Behm, S.M., 1991. A microorifice Uniform Deposit impactor (MOUDI): description, calibration, and use. Aerosol Sci. Technol. 14, 434–446.

Matthaios, M., Lawrence, J., Martins, M.A.G., Ferguson, S.T., Wolfson, J.M., Harrison, R. M., Koutrakis, P., 2022. Quantifying factors affecting contributions of roadway exhaust and non-exhaust emissions to ambient PM10–2.5 and PM2.5–0.2 particles. Sci. Total Environ. 835, 155368.

Men, Z., Zhang, X., Peng, J., Zhang, J., Fang, T., Guo, Q., Wei, N., Zhang, Q., Wang, T., Wu, L., Mao, H., 2022. Determining factors and parameterization of brake wear particle emission. J. Hazard Mater. 434, 128856.

Met Office, 2019. Met Office MIDAS Open: UK Land Surface Stations Data (1853-current). Centre for Environmental Data Analysis. https://catalogue.ceda.ac.uk/uu id/dbd451271eb04662beade68da43546e1. (Accessed 23 January 2023) [Last accessed.

Momenimovahed, A.D. Handford, Checkel, M.D., Olfert, J.S., 2015. Particle number emission factors and volatile fraction of particles emitted from on-road gasoline direct injection passenger vehicles. Atmos. Environ. 102, 105–111.

Mulani, S.M., Kumar, A., Naiyer, H., Shaikh, A., Saurabh, A., Singh, P.K., Verma, P.C., 2022. A review on recent development and challenges in automotive brake pad-disc system. Mater. Today Proc. 56 (2022), 447–454.

NAEI. UK, 2019. National Atmospheric Emissions Inventory. http://naei.beis.gov.uk/. (Accessed 23 January 2023) [Last accessed.

Oroumiyeh, F., Zhu, Y., 2021. Brake and tire particles measured from on-road vehicles: effects of vehicle mass and braking intensity. Atmos. Environ. X 12 100121.

Pant, P., Harrison, R.M., 2013. Estimation of the contribution of road traffic emissions to particulate matter concentrations from field measurements: a review. Atmos. Environ. 77, 78–97.

Park, J., Song, W., Gweon, J., Seo, H., Lee, J.J., Jang, H., 2021. Size effect of zircon particles in brake pads on the composition and size distribution of emitted particulate matter. Tribol. Int. 160, 106995.

Piscitello, A., Bianco, C., Casasso, A., Sethi, R., 2021. Non-exhaust traffic emissions: sources, characterization, and mitigation measures. Sci. Total Environ. 766, 144440.

Rivas, I., Beddows, D.C.S., Amato, F., Green, D.C., Järvi, L., Hueglin, C., Reche, C., Timonen, H., Fuller, G.W., Niemi, J.V., Pérez, N., Aurela, M., Hopke, P.K., Alastuey, A., Kulmala, M., Harrison, R.M., Querol, X., Kelly, F.J., 2020. Source apportionment of particle number size distribution in urban background and traffic stations in four European cities. Environ. Int. 135, 105345.

Song, W., Gweon, J., Park, J., Kwon, S.-U., Lee, J.J., Kim, Y.C., Jang, H., 2022. Effects of abrasive particles on the particulate matter emission of brake friction composites. Wear 504–505, 204436.

Tremper, A.H., Jephcote, C., Gulliver, J., Hibbs, L., Green, D.C., Font, A., Priestman, M., Hansell, A.L., Fuller, G.W., 2022. Sources of particle number concentration and noise near London Gatwick Airport. Environ. Int. 161, 107092.

Who, 2022. Ambient (Outdoor) Air Pollution. World Health Organisation. https://www.who.int/news-room/fact-sheets/detail/ambient-(outdoor)-air-quality-and-health. (Accessed 23 January 2023) [Last accessed.

Wu, H., Li, Z., Jiang, M., Liang, C., Zhang, D., Wu, T., Wang, Y., Cribb, M., 2021. Contributions of traffic emissions and new particle formation to the ultrafine particle size distribution in the megacity of Beijing. Atmos. Environ. 262, 118652.